HHS Public Access

Author manuscript

Nat Chem Biol. Author manuscript; available in PMC 2017 August 13.

Published in final edited form as:

Nat Chem Biol. 2017 April ; 13(4): 425–431. doi:10.1038/nchembio.2298.

AKAP-mediated feedback control of cAMP gradients in developing hippocampal neurons

Kirill Gorshkov[1,7], **Sohum Mehta**[7], **Santosh Ramamurthy**[2,3], **Gabriele V. Ronnett**[2,3,4,5], **Feng-Quan Zhou**[2,6], and **Jin Zhang**[1,7,*]

[1]Department of Pharmacology and Molecular Sciences, The Johns Hopkins University School of Medicine, Baltimore, MD 21205, USA

[2]Department of Neuroscience, The Johns Hopkins University School of Medicine, Baltimore, MD 21205, USA

[3]Center for Metabolism and Obesity Research, The Johns Hopkins University School of Medicine, Baltimore, MD 21205, USA

[4]Department of Neurology, The Johns Hopkins University School of Medicine, Baltimore, MD 21205, USA

[5]Department of Biological Chemistry, The Johns Hopkins University School of Medicine, Baltimore, MD 21205, USA

[6]Department of Orthopedic Surgery, The Johns Hopkins University School of Medicine, Baltimore, MD 21205, USA

[7]Department of Pharmacology, The University of California San Diego, La Jolla, CA 92093, USA

Abstract

Cyclic AMP (cAMP) and protein kinase A (PKA), classical examples of spatially compartmentalized signaling molecules, are critical axon determinants that regulate neuronal polarity and axon formation, yet little is known about micro-compartmentalization of cAMP and PKA signaling and its role in developing neurons. Here, we revealed that cAMP forms a gradient in developing hippocampal neurons, with higher cAMP levels in more distal regions of the axon compared to other regions of the cell. Interestingly, this cAMP gradient changed according to the developmental stage and depended on proper anchoring of PKA by A-kinase anchoring proteins (AKAPs). Disrupting PKA anchoring to AKAPs increased the cAMP gradient in early-stage neurons and led to enhanced axon elongation. Our results provide new evidence for a local

*Correspondence: Jin Zhang, 9500 Gilman Drive, BRF-II 1120, La Jolla, CA 92093-0702, phone (858) 246-0602, jzhang32@ucsd.edu.

Author Contributions

K.G. and S.R. performed the experiments; K.G., S.M. and J.Z. designed the experiments and interpreted the data. K.G., S.M. and J.Z. wrote the manuscript; K.G., S.R., S.M. and J.Z. edited the manuscript. Experiments were performed in the laboratories of G.R. and J.Z. FQ.Z. and J.Z. came up with the initial concept of the paper.

Competing Financial Interests

The authors declare no conflict of interest during the preparation of this manuscript.

negative feedback loop, assembled by AKAPs, for the precise control of a growth-stage-dependent cAMP gradient to ensure proper axon growth.

Keywords

FRET biosensors; neurodevelopment; signaling; second messengers; signalosome

Introduction

Neuronal development is an intricate, multi-stage process[1] in which the transition from progenitor cell to fully developed neuron depends on spatiotemporally regulated signaling events. Polarized growth is a particularly crucial aspect of this process, with individual neurons relying on coordinated pathways to ensure the proper development of a spatially distinct axon and dendrites[2]. Among these, 3′5′ cyclic adenosine monophosphate (cAMP) signaling, a pathway that is essential for many neuronal functions[3], is known to be a critical axon determinant[4].

cAMP is generated by adenylyl cyclases (ACs) and degraded by phosphodiesterases (PDEs); the free cAMP concentration in the cell is therefore dictated by the balance of these enzymatic activities. cAMP then binds and activates effector proteins such as protein kinase A (PKA) and exchange protein activated by cAMP (Epac), which play crucial roles in developing axons. For example, BDNF has been shown to elevate cAMP/PKA activity in the axon, leading to additional BDNF release and increased plasma membrane insertion of the BDNF receptor, TrkB, resulting in continued cAMP/PKA signaling and effectively generating a nested positive feedback loop in the nascent axon[5]. Similarly, Epac activation was shown to result in increased growth cone turning and neurite outgrowth, as well as axon regeneration in DRG neurons[6]. In hippocampal neurons (HNs), Epac regulates axon elongation via the activation of Rap1B and the subsequent activation of PI3K[7]. PKA and Epac have also been shown to play opposing roles. For example, in embryonic DRG neurons, growth cone attraction to morphogens was shown to be mediated by Epac, while repulsion was mediated by PKA[8].

cAMP signaling specificity is often achieved by confining cAMP elevations to discrete subcellular compartments[9, 10]. For example, asymmetric cAMP signaling can directly influence the formation of a single axon and multiple dendrites. Specifically, axonal cAMP elevations were found to have long-range inhibitory effects on dendritic cAMP levels in HNs, with the local elevation of cAMP at a nascent neurite leading to decreased cAMP levels in the remaining neurites[11]. Compartmentalization of the cAMP signaling machinery itself[12, 13] can further refine the spatial control of cAMP dynamics to modulate cell physiology. Adenylyl cyclase 5 (AC5), for example, was previously shown to be enriched in the distal axon and growth cone[14]. Nevertheless, cAMP dynamics have not been systematically examined in subcompartments of developing neurons.

At the PKA level, spatial compartmentalization is directly controlled by A-kinase anchoring proteins (AKAPs)[15–17], with many different AKAPs acting as scaffolds for the PKA holoenzyme, adenylyl cyclases, phosphodiesterases, phosphatases, and ion channels[18]. The

AKAP microdomain localizes the regulators and effectors of PKA signaling and serves to spatially control PKA function by binding the RII subunit of PKA[19], the major regulatory subunit in neurons[20]. Thus, any PKA signaling that contributes to the initiation of morphological compartmentation exists within a scaffold of PKA regulators and effectors[21]. However, despite efforts to understand the role of AKAPs in neuronal excitability and synaptic responses[3, 18], there has not been significant inquiry into the role AKAPs play in neuronal development.

Here, we utilized genetically encoded fluorescence resonance energy transfer (FRET)-based biosensors to investigate cAMP/PKA signaling dynamics in stage-three to stage-four primary rat HNs[22]. Neurons at these stages have nascent and spatially distinct dendrites and axons in the process of elongation. Using these probes, we uncovered a developmentally timed, axon-directed cAMP gradient that is maintained by AKAP-anchored PKA activity and that is critical for ensuring proper axonal development. Our results suggest that, although cAMP and PKA are widely regarded as playing a positive role in promoting and establishing neuronal polarity, axon elongation, and guidance[8, 14, 23–25], these signaling molecules in fact play a more nuanced role in shaping neuronal development than previously appreciated.

Results

Stage-specific cAMP signaling in developing HNs

The stages of neuronal development can be defined *in vitro* by plating HNs onto polylysine-coated glass coverslips.[1, 26] Between the time of plating and 7 days in culture, neurons proceed through five main stages of growth. At stage one (0 h), the neuron is uniform in shape, with small, lamellar protrusions extending from the cell body. At stage two (12 h), the neuron forms immature neurites. At stage three (36 h), the cell begins to specify the fate of one of these neurites to grow rapidly and form the axon. At stage four (4 days), the dendrites begin to grow. At stage five and beyond (>7 days), the neuron begins to mature. We therefore used rat (*Rattus norvegicus*) HNs grown for five days *in vitro* (DIV5) to investigate the molecular activities involved in neurite outgrowth.

We first used the genetically encoded FRET-based cAMP biosensor ICUE3 (Fig. 1a)[27] to analyze the activity and regulation of cAMP in living neurons. ICUE3 contains a truncated version of Epac1 (aa 149–881) sandwiched between ECFP (donor) and cpVenus-L194 (acceptor), wherein the binding of cAMP results in a conformational change in this truncated Epac1 and an increase in the donor-to-acceptor (C/Y) emission ratio. Using this probe, we observed a range of emission ratio changes in different regions of DIV5 HNs upon bath stimulation with 50 μM forskolin (Fsk), a general activator of transmembrane ACs; on average, the ratio increases were significantly lower in the soma, dendrites, and proximal axon (21.8±3.7%, 24.5±3.7%, and 30.6±5.0%, respectively) than in the middle and distal axon (41.8±5.3% and 47.8±5.7%; mean±SEM, n=12) (Fig. 1b–d), which showed no difference in diameter (Supplementary Results, see Supplementary Fig. 1 online), indicating the presence of a gradient of cAMP signaling towards the axon in these cells. These data are consistent with previously suggested axonal-dendritic differences in cAMP[14] and further define axonal subcompartments that show distinct cAMP characteristics.

Although axonal-dendritic differences in cAMP have previously been suggested to assist in neuronal development[5, 11], cAMP gradients have yet to be investigated at different stages of development. We therefore compared the cAMP dynamics of DIV5 HNs with those of less-developed DIV3 HNs. Overall, we observed a weaker and more uniform ICUE3 response to Fsk stimulation in DIV3 cells compared with that in DIV5 cells, with a gradual increase of ~15% over 20 min and no significant differences in the different cellular regions (Fig. 1e–g). Thus, neurons at different developmental stages have different capacities for generating cAMP gradients.

Because such capacities originate from balanced actions of ACs and PDEs[28], we next tested the role of PDEs in generating the cAMP gradient observed in DIV5 cells. Interestingly, treatment with the general PDE inhibitor 3-isobutyl 1-methylxanthine (IBMX) revealed a weak axon-directed cAMP response in these cells (see Supplementary Fig. 2 online), with subsequent Fsk stimulation producing a large, uniform ratio increase of ~50–60% (see Supplementary Fig. 2 online). DIV3 HNs treated with IBMX similarly exhibited a small, axon-directed increase in cAMP (see Supplementary Fig. 2 online), followed by a larger, uniform increase in emission ratio upon Fsk stimulation (see Supplementary Fig. 2 online). Treatment with the isoform-specific inhibitors rolipram (PDE4 specific) and milrinone (PDE3 specific) followed by Fsk revealed that PDE4 is the dominant isoform at DIV3, as well as at DIV5, as rolipram pretreatment mimicked the effect of IBMX on potentiating the Fsk-induced response, in contrast to milrinone pretreatment (see Supplementary Fig. 3 online). Collectively, these data reveal differences in cAMP signaling within neuronal compartments and between HNs at different developmental stages. Specifically, both DIV3 and DIV5 HNs displayed higher AC activity towards the axon, yet DIV3 HNs appeared to possess stronger PDE activity compared with DIV5 HNs. Our results suggest that this imbalance in favor of PDE activity contributes to the lower stimulated cAMP production observed in newly polarized, DIV3 cells. On the other hand, despite a lack of clear spatial differences in the distribution of AC or PDEs in either DIV3 or DIV5 HNs (Supplementary Fig. 4 online), the lower axonal PDE activity in DIV5 HNs may allow polarized AC activity to induce the formation of a steep cAMP gradient, with higher cAMP levels in more distal regions of the axon compared to other regions of the cell.

Spatially distinct PKA activity in developing HNs

Because PKA is directly downstream of cAMP, and because several isoforms are clearly present in these HNs (see Supplementary Fig. 5 online), we wanted to know if PKA activity follows the axon-directed cAMP gradient observed above. We therefore transfected DIV5 and DIV3 HNs with the PKA activity biosensor AKAR4[9], which contains a PKA substrate sequence and phosphoamino acid-binding domain (FHA1) sandwiched between Cerulean (donor) and cpVenus-E172 (acceptor) and reports on PKA activity via increases in the acceptor-to-donor (Y/C) emission ratio (see Supplementary Fig. 6 online). However, AKAR4-expressing DIV5 and DIV3 HNs both responded to 50 μM Fsk stimulation with uniform FRET ratio increases (~40%) among all the regions (see Supplementary Fig. 6 online). Cells expressing a negative-control reporter (AKAR4-TA), in which the target Thr is mutated to Ala, showed no response to 50 μM Fsk, confirming that these responses are due to phosphorylation of the reporter (see Supplementary Fig. 7 online). Subsequent treatment

with 100 μM IBMX failed to elicit any additional increase in both DIV5 and DIV3 cells (see Supplementary Fig. 6 online), indicating that the AKAR4 response was fully saturated.

Because cAMP binds to PKA with an ~1000 fold higher affinity compared with Epac[29], we suspected that the saturating effect of 50 μM Fsk stimulation was masking the underlying spatial differences in PKA activity. We therefore tested whether submaximal stimulation would reveal a PKA gradient. Indeed, treating DIV5 cells with one-hundredfold less (500 nM) Fsk generated an axon-directed PKA activity gradient that paralleled the cAMP response (Fig. 2a,b; left). On the other hand, DIV3 cells showed only small (~5%) responses to the low dose of Fsk, with no significant differences between the regions (Fig. 2a,b; right). Pretreating DIV3 HNs with IBMX resulted in an ~40% ratio increase in response to 500 nM Fsk, whereas IBMX treatment alone produced an ~50% ratio increase in DIV5 HNs, confirming that the reporter was functioning normally (Fig. 2c). Representative cells are illustrated in Fig. 2d.

We also observed a clear, axon directed gradient in the AKAR4 starting ratio in DIV5 HNs (see Supplementary Fig. 8 online). Although control cells expressing AKAR4-TA also exhibited higher starting ratios in the distal axon, possibly due to slightly higher levels of the probe in this region, the starting ratio differences were steeper with AKAR4 than with AKAR4-TA in DIV5 HNs (see Supplementary Fig. 8 online), whereas both AKAR4 and AKAR4-TA exhibited similar starting ratio differences in DIV3 HNs (see Supplementary Fig. 8 online), suggesting the presence of a bona fide gradient of basal PKA activity in resting DIV5 HNs. These data indicate that PKA follows the cAMP response pattern seen in DIV5 HNs, with an axon-directed gradient of PKA activity, whereas more immature HNs lack such a gradient.

AKAP anchoring modulates basal PKA activity in axons

AKAP anchoring plays an important role in spatially restricting PKA in cells. The presence of various AKAPs in these HNs (see Supplementary Fig. 9 online) prompted us to investigate whether the PKA gradient in DIV5 HNs depends on AKAP anchoring. To this end, we treated cells with a cell-permeable form of Ht31 (st-Ht31), a peptide derived from AKAP-Lbc[30, 31] that is known to disrupt PKA RII binding to AKAPs. In DIV5 HNs, st-Ht31 treatment led to a minimal change in the PKA activity within the somatodendritic compartment and a larger decrease in the axonal regions (Fig. 3a,b; left). On the other hand, DIV3 HNs exhibited no significant change in PKA activity among the different regions (Fig. 3a,b; right) following st-Ht31 treatment. DIV5 HNs transfected with the negative-control reporter exhibited no change upon st-Ht31 treatment (see Supplementary Fig. 10 online). Representative cells are illustrated in Fig. 3c. These results further support our conclusion that the starting ratio differences in DIV5 HNs correspond to differential PKA activity and reveal that the axonal PKA gradient is promoted by AKAP anchoring.

Delocalizing PKA enhances axon elongation in immature HNs

We next investigated the functional role of AKAP-mediated PKA compartmentalization in axon development. PKA plays a well-known role in promoting axonogenesis[24, 32, 33], and AKAP anchoring promotes the specificity of PKA signaling in part by localizing PKA near

its downstream substrates. Thus, we hypothesized that the AKAP anchoring of PKA would have a pro-axonogenic effect in developing HNs. To test this hypothesis, we treated newly plated HNs (16–20 h *in vitro*) with st-Ht31 to disrupt AKAP-PKA anchoring and then performed immunostaining to detect Tau1, an axon-specific marker, as well as MAP2, a dendrite specific marker, after 72 h *in vitro* (DIV3) (Fig. 4a). Axon growth was assessed by measuring the length of the longest Tau1-positive neurite extending from the soma of each cell (Fig. 4b–i). Based on the reported positive role of PKA in axon development, we expected the disruption of PKA anchoring to have a detrimental effect on axon outgrowth. Surprisingly, however, we observed significantly longer neurites in DIV3 HNs treated with st-Ht31 compared with control HNs treated with DMSO, and treatment with a scrambled peptide (st-Ht31p) had no effect on neurite length (Fig. 4b–e). Furthermore, PKA inhibition by either H89, KT5720, or Rp-8-Br-cAMPS had no effect on axon elongation (Fig. 4f–h). The enhancement of neurite outgrowth with st-Ht31 was also dose dependent, with increasing doses of st-Ht31 progressively increasing neurite length (see Supplementary Fig. 11 online).

AKAP disruption enhances the cAMP gradient in DIV3 HNs

Combined with our previous observation that axonal PKA activity is supported by AKAP anchoring, the fact that disrupting the PKA-AKAP microdomain enhances axon elongation suggests that AKAP-anchored PKA acts to limit axon elongation during early developmental timepoints. These results are surprising because cAMP and PKA are thought to promote axon polarization and elongation and because AKAP anchoring helps support PKA function. We therefore investigated whether the st-Ht31 effect on axon length was related to the observed spatial differences in cAMP signaling. To this end, we treated ICUE3-expressing DIV3 HNs with st-Ht31 followed by Fsk. The addition of st-Ht31 yielded small increases in cAMP levels, with a slightly larger increase in the axon, and subsequent stimulation with Fsk produced a steep, axon-directed cAMP gradient (Fig. 5a–c). Comparing the Fsk-induced ICUE3 response in DIV3 HNs with and without st-Ht31 pretreatment revealed a significant difference in cAMP levels in the middle and distal axon (Fig. 5d). In fact, this gradient was very similar to that observed in DIV5 HNs treated with Fsk alone (Fig. 5d). Meanwhile, st-Ht31 treatment appeared to increase somatodendritic cAMP accumulation yet had no effect on axon length in more mature HNs (see Supplementary Fig. 12 and 13 online). These data imply that delocalizing PKA from the AKAP microdomain specifically enhances cAMP accumulation in DIV3 HNs, especially in more distal regions of the axon. Hence, younger neurons with delocalized PKA exhibited cAMP gradients typically seen only in older neurons.

Developmentally regulated cAMP signaling in HNs

Our results suggest that PKA acts as a local negative-feedback regulator of cAMP signaling within an AKAP microdomain in developing neurons. Indeed, we found that directly inhibiting PKA also increased cAMP in the axon of DIV3 HNs (see Supplementary Fig. 14 online), further suggesting that PKA activity has a negative effect on cAMP levels in these cells. Two possible mechanisms could explain this effect: the PKA-mediated inhibition of ACs such as AC V and VI[34, 35] or the PKA-mediated activation of PDEs such as PDE4[36]. However, the fact that PDE inhibition revealed elevated axonal cAMP levels in DIV3 HNs

(see Supplementary Fig. 2 online) is inconsistent with a model of local AC inhibition, which would instead predict either the absence of a gradient or lower axonal cAMP levels following PDE inhibition. Furthermore, comparing the responses of ICUE3-expressing DIV3 HNs to IBMX, H89, and st-Ht31 indicated that the cAMP response to PDE inhibition was qualitatively similar to the axon-directed cAMP gradient produced by either inhibiting or delocalizing PKA (Fig. 5e). The cAMP gradient was steeper following both AKAP disruption and PKA inhibition compared with PDE inhibition (see Supplementary Fig. 15 online), which is consistent with the targeted disruption of local PKA-PDE feedback versus more general inhibition. Thus, our data support a model (Fig. 5f) in which PKA and PDE form an AKAP-anchored signaling microdomain in the developing axon of immature (e.g., DIV3) HNs. Basally active PKA phosphorylates and activates co-anchored PDE, which locally degrades cAMP, thereby forming a negative feedback loop that dampens axonal cAMP signaling and limits axon elongation. Disrupting this AKAP-anchored feedback circuit leads younger cells to mimic more mature (e.g., DIV5) HNs, in which the feedback circuit is absent, by prematurely forming an axon-directed cAMP gradient that drives axon elongation.

Discussion

cAMP/PKA signaling is essential to neuronal development and growth. Some of the earliest studies on the role of cAMP in axon biology focused on axon guidance, indicating that local sources of cAMP can act as attractants for growth cones[23, 37]. Recent work on axon formation also showed that neurons prefer to grow axons on cAMP-laden stripes and are repelled by stripes containing inhibitory cAMP analogs or PKA inhibitors[11], while individual neurites exposed to a local source of cAMP tended to turn into axons rather than dendrites. Our investigation revealed growth stage-specific cAMP gradients and suggests that a steeper cAMP gradient is correlated with enhanced axon elongation. These findings are in keeping with past observations of spatially regulated cAMP signaling during axon development, such as local elevations in cAMP within the growth cones of *Xenopus* spinal neurons[38]. Although local signaling events can often be driven by the spatial distribution of signaling factors such as ACs[14], our analyses did not reveal any clear spatial differences in the distribution of AC or PDEs in either DIV3 or DIV5 HNs that could give rise to the signaling patterns observed in the present study.

The geometry of neuronal subcompartments has also been shown to play a role in determining local cAMP concentrations, which can help explain the generation of gradients in thin processes. Modeling work in recent years has revealed that molecules such as cAMP can become concentrated in compartments with high surface-to-volume ratios, i.e., thinner processes, as the rate of production generally exceeds that of diffusion in these thin compartments[39]. Furthermore, concentration is also positively correlated with increasing distance from the soma[39]. In fact, dendritic geometry has been shown to counteract the effects of increasing distance from the soma to enhance cAMP-dependent nuclear signaling[40]. In our study, we found no obvious correlation between distance from the soma and axonal diameter in ICUE3-expressing DIV5 neurons (see Supplementary Fig. 1 online), suggesting that the gradient of cAMP accumulation that we observed in these cells is not significantly influenced by axonal geometry.

Our findings also complicate the role of PKA in axonogenesis. Previously, PKA-dependent phosphorylation of LKB1 was shown to promote axon formation both *in vitro* and *in vivo* through the activation of SAD kinases[24, 33, 41], which show elevated activity in the distal axon[42]. In the present study, we observed that disrupting PKA compartmentalization in DIV3 HNs not only led to higher axonal cAMP but also increased axon elongation. On the other hand, AKAP disruption had no effect on axon length in DIV5 HNs, despite causing an apparent increase in somatodendritic cAMP accumulation. These results suggest a specific role for axonal PKA activity in blocking axon elongation in immature HNs, which is a departure from the established, exclusively positive role of PKA in axon development. It is possible that axonal PKA in fact plays a dual role as both a positive and negative regulator of axon elongation through LKB1 and cAMP, respectively. This complexity may account for the lack of observed effects on axon growth when PKA activity was inhibited directly, as both the negative and positive PKA pathways would be blocked. Furthermore, recent work has shown that Epac is also necessary for axon extension[43,7], and the increased cAMP levels caused by delocalizing PKA in developing HNs likely also enhance axon outgrowth through the activation of Epac. Indeed, PKA and Epac1 were both clearly expressed in these cells (see Supplementary Fig. 5 online), and experiments performed using ESI-09, an Epac1-specific inhibitor, confirm the critical role of Epac signaling in axon outgrowth in developing hippocampal neurons.

The effects of delocalizing PKA using st-Ht31 specifically highlight the importance of AKAP-compartmentalized PKA activity in developing HNs, and are consistent with previous findings of PKA compartmentalization within specific neuronal structures[44]. AKAPs often act to facilitate PKA signaling by colocalizing PKA with downstream targets[1545] and by coupling PKA activity to specific upstream signals[46]. However, AKAP anchoring can also play a major role in shaping the dynamics of both PKA and cAMP signaling by localizing PKA with regulatory proteins such as PDEs[47,48], and our results indicate that this type of “regulatory” AKAP microdomain is central to directing the course of axon elongation in developing HNs. For instance, AKAP12/Gravin, which binds both PKA and PDE4D, can be found throughout mouse HNs[49] and in punctate structures in NT2-N human model neurons[50]. Another PKA/PDE4D3 scaffold, AKAP9 can assemble signaling platforms on centrosomes, and its splice variant Yotiao has also been shown to bind NMDA subunits[51], although Yotiao has not been shown to bind to PDEs. Interestingly, WAVE-1 knockout mice exhibit clear changes in brain structure and behavioral deficits[52], and knocking down WAVE-1 in HNs reduces axon length[53]; however, WAVE-1 has also not been demonstrated to bind PDEs. Lastly, mAKAP, which binds Epac1, PKA, PDE4D3 and ACs, has been found to promote axon elongation and survival in injured retinal ganglion cells, but not during normal growth[54]. Nevertheless, the mAKAP signalosome may also play a role in coordinating cAMP signaling in different neuronal cell types, including HNs. However, while we were able to detect the expression of these and other AKAPs in DIV5 and DIV3 HNs, our initial analyses did not uncover any obvious differences in expression or localization that might explain the signaling differences between these developmental stages. It therefore remains to be seen which specific AKAP is responsible for the localized effects observed in our study.

Our work using cultured rat HNs as a model system has established the functional relevance of AKAP-mediated cAMP/PKA compartmentalization in neuronal differentiation and development. Future studies of the various AKAPs will help drive our understanding of cAMP signaling regulation in neuronal development.

Online Methods

Reagents

Papain Dissociation System was purchased from Worthington (Lakewood, NJ). Neurobasal was purchased from Invitrogen (21103-049). B27 was purchased from Gibco (17504044). Pen-Strep was purchased from Thermo-Fisher (15140122). GlutaMax was purchased from Gibco (35050061). Poly-D-Lysine (PDL) was purchased from Sigma (P6407). Lipofectamine LTX was purchased from Invitrogen (15338030). Forskolin (Fsk, 344270) and 3-isobutyl-1-methylxanthine (IBMX, 410957) were purchased from Calbiochem and used at a final concentration of 500 nM or 50 μM (Fsk) and 100 μM (IBMX)[55, 56, 57]. H89 was purchased from Sigma (B1427) and used at a concentration of 10 μM[58, 59]. KT5720 (K7361), Rp-8-Br-cAMPS (B1381), and ESI-09 (SML0814) were purchased from Sigma. St-Ht31 (V8211) and st-Ht31p (V8221) were purchased from Promega. Paraformaldehyde solution (16%) was purchased from Electron Microscopy Sciences (15700, 4% final dilution). Rabbit anti-Tau1 (ab64193, 1:100 dilution) and mouse anti-NST (ab14545, 1:1000 dilution) were purchased from Abcam. Mouse-anti MAP2 (1:500, MAB3418) was purchased from Millipore. Rabbit anti-AKAP79 (1:100, sc10764), rabbit anti-AKAP95 (1:100, sc10766), rabbit anti-PDE3B (1:100, sc-20793), rabbit anti-PDE4D (1:100, sc-25814) and mouse anti-Epac (1:100, sc-28366) were purchased from Santa Cruz Biotechnology. Mouse anti-AKAP9 (1:100, NB100-74351) was purchased from Novus Biological. Mouse anti-WAVE 1 (1:100, ab106516) and rabbit anti-ADCY5/6 (1:100, ab196748) were purchased from Abcam. Rabbit anti-PKA (Cα) (1:100, ab4782) was purchased from Cell Signaling Technologies. Mouse anti-PKA RIIβ (1:100, 610625) and mouse anti-PKA RIα (1:100, 610165) were purchased from BD Biosciences. Goat anti-mouse Alexa-Fluor 488 (A-11001, 1:1000 dilution) and goat anti-rabbit Alex-Fluor 568 (A-11036, 1:1000 dilution) were purchased from Thermo Fisher Scientific. Prolong Gold antifade mounting reagent was purchased from Life Technologies (P36930).

Cell Culture

Primary rat hippocampal neurons - Hippocampi were dissected from E18 Sprague Dawley rat (*Rattus norvegicus*) pups (Harlan) in ice-cold Hank's Balanced Salt Solution (HBSS) supplemented with 20 mM HEPES, pH 7.4, 5 mM D-glucose, 0.23 mM sodium pyruvate, and 0.5% pen-strep and were dissociated using the Papain Dissociation System according the manufacturer's instructions. Dissociated HNs were re-suspended in Neurobasal medium supplemented with 2.0% B27 supplement, 0.5% pen-strep and 2.0 mM Glutamax. Each separate preparation contained pooled tissues from a single litter (~10–12 pups), with one preparation performed per week. Approximately 1.0×10^5 cells were plated onto 35-mm nitric acid-treated glass-bottom imaging dishes coated with 150 μg/mL PDL. Cells were given a 50% media change every three days to restore glucose levels to 3.0 mM as previously described[60]. Cells were cultured at 37°C in a humidified incubator at 5% CO_2. At

DIV2 or DIV4, cells were transfected with Lipofectamine LTX according to manufacturer's instructions and imaged after 24 h.

Live-cell Imaging

Cells were washed twice with HBSS prior to imaging and maintained in the dark at 37°C. DMSO, Fsk, IBMX, H89 and st-Ht31 were added as indicated. Dual emission ratio imaging was performed on a Zeiss AxioObserver Z1 microscope (Carl Zeiss) equipped with a 40x/1.3 NA objective and a Photometrics Evolve 512 EMCCD (Photometrics) controlled by METAFLUOR 7.7 software (Molecular Devices). Images were acquired using a 420DF20 excitation filter, a 450DRLP dichroic mirror, and two emission filters (475DF40 for CFP and 535DF25 for YFP) alternated by a Lambda 10-2 filter-changer (Sutter Instruments). Exposure times ranged between 50 and 500 ms, and images were acquired every 30 s.

Images were analyzed in METAFLUOR 7.7 by defining a single region of interest (ROI) for the dendrites and for the soma, with the axon separated into three equal-length ROIs of ~40–50 μm (see Supplementary Fig. 16 online). The proximal axon region is defined as the length of axon extending directly from the soma, and the middle and distal axon regions correspond to the next two equal-length segments after the proximal segment. The same axon segments were analyzed for both DIV3 and DIV5 HNs. Only one cell could be imaged per dish, and data were averaged across multiple independent dishes and across multiple cell preparations. Fluorescence images in each channel were background-corrected by subtracting the fluorescence intensity of an ROI corresponding to a background region with no cells from the emission intensities of cells expressing fluorescent biosensors. The biosensors used in this study contain cyan fluorescent protein (CFP) as the donor and yellow fluorescent protein (YFP) as the acceptor. Three channels were captured per image acquisition: CFP (direct donor excitation and emission), YFP-FRET (donor-sensitized acceptor emission), and YFP (direct acceptor excitation and emission). ICUE3 uses $Epac1^{149–881}$ as the sensing domain and eCFP/cpV-L194 as the FRET pair. Emission ratios (CFP/YFP-FRET) for ICUE3 and (YFP-FRET/CFP) for AKAR4 were then calculated for the different ROIs at each timepoint. Emission ratios were normalized by dividing the ratio at each timepoint by the value immediately before drug addition. Pseudocolor ratiometric images were scaled to the indicated upper and lower bounds for emission ratios. For ICUE3, warmer colors indicate higher C/Y ratios. For AKAR4, warmer colors indicate higher Y/C ratios. In some cases, the cell body of the neuron is brighter than the rest of the cell and therefore appears black or pink. The color of the soma is not an indication of intensity saturation. The pseudocolor images were not used for data analysis.

Immunocytochemistry

Approximately $2.0×10^4$ HNs were cultured on nitric acid-washed, PDL-coated 15-mm glass coverslips for ~16–20 h, treated with the indicated drugs, and cultured for an additional 48 h. At DIV3, cells were fixed with 4% PFA for 20 min at room temperature. Free PFA was quenched with 100 mM glycine in HBSS. Cells were then permeabilized and preincubated in blocking buffer (5% goat serum, 0.2% BSA, 0.1% Triton-X 100, and 0.01% NaN_3 in HBSS) for 30 min. The cells were incubated overnight at 4°C with the following primary antibodies in blocking buffer: rabbit Tau1 and mouse NST. On the following day, the cells

were washed 3 times in HBSS and incubated with goat anti-rabbit Alexa-Fluor-568 or goat anti-mouse Alexa-Flour-488 secondary antibody for 2 h at room temperature in the dark. Cells were then washed once with HBSS, counterstained with 1 mg/mL Hoechst stain to visualize the nuclei, and washed another 3 times with HBSS. Prolong Gold anti-fade mounting reagent was used to mount coverslips for imaging on a Zeiss LSM700 inverted confocal microscope (Carl Zeiss). All images were processed using ImageJ software (NIH) and the Simple Neurite Tracer plugin.

Statistical Analysis

Graphs were plotted using GraphPad Prism 6 (GraphPad), and all statistical analyses were performed using the same software. Sample size was not predetermined prior to performing the experiments. Cells were excluded from data acquisition when axons and dendrites were not obviously developed. Pairwise comparisons were performed using two-sided Student's t-test, and statistical significance was set at $p<0.05$. Global comparisons of sensor responses were performed using one- or two-way ordinary ANOVA analysis, and statistical significance was set at $p<0.05$. Following the two-way ANOVA, a Dunnet's multiple comparison test was used for determining statistical significance between individual conditions. Bar graphs depict the mean±S.E.M. For box-and-whisker plots, the box shows the median, 25% quartile, and 75% quartile, and the whiskers designating the 5th and 95th percentiles; the mean value is indicated with a "+". Investigators were not blinded to the group allocation during analysis.

Data Availability

Data sets are available upon request.

Supplementary Material

Refer to Web version on PubMed Central for supplementary material.

Acknowledgments

We thank Drs. Randal Hand and Alex Kolodkin from Johns Hopkins School of Medicine Department of Neuroscience for consultation on various aspects of this manuscript, reagents, and microscopy training. We thank the Malinow lab and Irina Hunton at the University California San Diego for use of their lab space and coordinating dissections. We thank Zhang Lab members, especially Dr. Eric Greenwald, for discussions. This work was supported by the UCSD Neuroscience Microscopy Shared Facility Grant P30 NS047101, NSF GRF 1232825 (to K.G.), DGIST Convergence Science Center grant 11-BD-04 (to G.V.R.), R01NS085176 and the Craig H. Neilsen Foundation to (FQ.Z.), and NIH R01 DK073368 (to J.Z.).

References

1. Dotti C, Sullivan C, Banker G. The establishment of polarity by hippocampal neurons in culture. The Journal of Neuroscience. 1988; 8:1454–1468. [PubMed: 3282038]
2. Barnes AP, Polleux F. Establishment of axon-dendrite polarity in developing neurons. Annu Rev Neurosci. 2009; 32:347–381. [PubMed: 19400726]
3. Park AJ, et al. A presynaptic role for PKA in synaptic tagging and memory. Neurobiology of Learning and Memory. 2014; 114:101–112. [PubMed: 24882624]
4. Pasterkamp RJ. Getting neural circuits into shape with semaphorins. Nat Rev Neurosci. 2012; 13:605–618. [PubMed: 22895477]

5. Cheng PL, et al. Self-amplifying autocrine actions of BDNF in axon development. Proceedings of the National Academy of Sciences of the United States of America. 2011; 108:18430–18435. [PubMed: 22025720]
6. Murray AJ, Shewan DA. Epac mediates cyclic AMP-dependent axon growth, guidance and regeneration. Molecular and Cellular Neuroscience. 2008; 38:578–588. [PubMed: 18583150]
7. Muñoz-Llancao P, et al. Exchange Protein Directly Activated by cAMP (EPAC) Regulates Neuronal Polarization through Rap1B. The Journal of Neuroscience. 2015; 35:11315–11329. [PubMed: 26269639]
8. Murray AJ, Tucker SJ, Shewan DA. cAMP-Dependent Axon Guidance Is Distinctly Regulated by Epac and Protein Kinase A. The Journal of Neuroscience. 2009; 29:15434–15444. [PubMed: 20007468]
9. Depry C, Allen MD, Zhang J. Visualization of PKA activity in plasma membrane microdomains. Molecular BioSystems. 2011; 7:52–58. [PubMed: 20838685]
10. Gervasi N, et al. Dynamics of protein kinase A signaling at the membrane, in the cytosol, and in the nucleus of neurons in mouse brain slices. The Journal of neuroscience : the official journal of the Society for Neuroscience. 2007; 27:2744–2750. [PubMed: 17360896]
11. Shelly M, et al. Local and Long-Range Reciprocal Regulation of cAMP and cGMP in Axon/Dendrite Formation. Science. 2010; 327:547–552. [PubMed: 20110498]
12. Nikolaev VO, et al. Beta2-adrenergic receptor redistribution in heart failure changes cAMP compartmentation. Science. 2010; 327:1653–1657. [PubMed: 20185685]
13. Castro LR, et al. Type 4 phosphodiesterase plays different integrating roles in different cellular domains in pyramidal cortical neurons. The Journal of neuroscience : the official journal of the Society for Neuroscience. 2010; 30:6143–6151. [PubMed: 20427672]
14. del Puerto A, et al. Adenylate cyclase 5 coordinates the action of ADP, P2Y1, P2Y13 and ATP-gated P2X7 receptors on axonal elongation. Journal of Cell Science. 2012; 125:176–188. [PubMed: 22250198]
15. Murphy, Jonathan G., et al. AKAP-Anchored PKA Maintains Neuronal L-type Calcium Channel Activity and NFAT Transcriptional Signaling. Cell Reports. 2014; 7:1577–1588. [PubMed: 24835999]
16. Esseltine JL, Scott JD. AKAP signaling complexes: pointing towards the next generation of therapeutic targets? Trends in Pharmacological Sciences. 2013; 34:648–655. [PubMed: 24239028]
17. Sanderson JL, Dell'Acqua ML. AKAP Signaling Complexes in Regulation of Excitatory Synaptic Plasticity. The Neuroscientist. 2011; 17:321–336. [PubMed: 21498812]
18. Carnegie GK, Scott JD. A-kinase anchoring proteins and neuronal signaling mechanisms. Genes & development. 2003; 17:1557–1568. [PubMed: 12842908]
19. Carr DW, Hausken ZE, Fraser ID, Stofko-Hahn RE, Scott JD. Association of the type II cAMP-dependent protein kinase with a human thyroid RII-anchoring protein. Cloning and characterization of the RII-binding domain. J Biol Chem. 1992; 267:13376–13382. [PubMed: 1618839]
20. Ventra C, et al. The Differential Response of Protein Kinase A to Cyclic AMP in Discrete Brain Areas Correlates with the Abundance of Regulatory Subunit II. Journal of Neurochemistry. 1996; 66:1752–1761. [PubMed: 8627334]
21. Taylor SS, Zhang P, Steichen JM, Keshwani MM, Kornev AP. PKA: Lessons Learned after Twenty Years. Biochimica et biophysica acta. 2013; 1834:1271–1278. [PubMed: 23535202]
22. Gorshkov K, Zhang J. Visualization of cyclic nucleotide dynamics in neurons. Frontiers in cellular neuroscience. 2014; 8doi: 10.3389/fncel.2014.00395
23. Lohof A, Quillan M, Dan Y, Poo M. Asymmetric modulation of cytosolic cAMP activity induces growth cone turning. The Journal of Neuroscience. 1992; 12:1253–1261. [PubMed: 1372932]
24. Shelly M, Cancedda L, Heilshorn S, Sumbre G, Poo M-m. LKB1/STRAD Promotes Axon Initiation During Neuronal Polarization. Cell. 2007; 129:565–577. [PubMed: 17482549]
25. Song, H-j, Ming, G-l, Poo, M-m. cAMP-induced switching in turning direction of nerve growth cones. Nature. 1997; 388:275–279. [PubMed: 9230436]
26. Goslin K, Banker G. Experimental observations on the development of polarity by hippocampal neurons in culture. J Cell Biol. 1989; 108:1507–1516. [PubMed: 2925793]

27. DiPilato LM, Zhang J. The role of membrane microdomains in shaping [small beta]2-adrenergic receptor-mediated cAMP dynamics. Molecular BioSystems. 2009; 5:832–837. [PubMed: 19603118]
28. Dessauer CW. Adenylyl Cyclase–A-kinase Anchoring Protein Complexes: The Next Dimension in cAMP Signaling. Molecular Pharmacology. 2009; 76:935–941. [PubMed: 19684092]
29. Dao KK, et al. Epac1 and cAMP-dependent Protein Kinase Holoenzyme Have Similar cAMP Affinity, but Their cAMP Domains Have Distinct Structural Features and Cyclic Nucleotide Recognition. Journal of Biological Chemistry. 2006; 281:21500–21511. [PubMed: 16728394]
30. Carr DW, Hausken ZE, Fraser ID, Stofko-Hahn RE, Scott JD. Association of the type II cAMP-dependent protein kinase with a human thyroid RII-anchoring protein. Cloning and characterization of the RII-binding domain. Journal of Biological Chemistry. 1992; 267:13376–13382. [PubMed: 1618839]
31. Vijayaraghavan S, Goueli SA, Davey MP, Carr DW. Protein Kinase A-anchoring Inhibitor Peptides Arrest Mammalian Sperm Motility. Journal of Biological Chemistry. 1997; 272:4747–4752. [PubMed: 9030527]
32. Bouchard JF, et al. Protein Kinase A Activation Promotes Plasma Membrane Insertion of DCC from an Intracellular Pool: A Novel Mechanism Regulating Commissural Axon Extension. The Journal of Neuroscience. 2004; 24:3040–3050. [PubMed: 15044543]
33. Barnes AP, et al. LKB1 and SAD Kinases Define a Pathway Required for the Polarization of Cortical Neurons. Cell. 2007; 129:549–563. [PubMed: 17482548]
34. Chen Y, et al. Adenylyl cyclase 6 is selectively regulated by protein kinase A phosphorylation in a region involved in Gα(s)-stimulation. Proceedings of the National Academy of Sciences of the United States of America. 1997; 94:14100–14104. [PubMed: 9391159]
35. Iwami G, et al. Regulation of adenylyl cyclase by protein kinase A. J Biol Chem. 1995; 270:12481–12484. [PubMed: 7759492]
36. Mika D, Conti M. PDE4D phosphorylation: A coincidence detector integrating multiple signaling pathways. Cellular signalling. 2015; 28:719–724. [PubMed: 26562185]
37. Song HJ, Ming GL, Poo MM. cAMP-induced switching in turning direction of nerve growth cones. Nature. 1997; 388:275–279. [PubMed: 9230436]
38. Nicol X, Hong KP, Spitzer NC. Spatial and temporal second messenger codes for growth cone turning. Proceedings of the National Academy of Sciences of the United States of America. 2011; 108:13776–13781. [PubMed: 21795610]
39. Neves SR, et al. Cell Shape and Negative Links in Regulatory Motifs Together Control Spatial Information Flow in Signaling Networks. Cell. 2008; 133:666–680. [PubMed: 18485874]
40. Li L, Gervasi N, Girault JA. Dendritic geometry shapes neuronal cAMP signalling to the nucleus. Nat Commun. 2015; 6:6319. [PubMed: 25692798]
41. Shelly M, Poo MM. Role of LKB1-SAD/MARK pathway in neuronal polarization. Developmental Neurobiology. 2011; 71:508–527. [PubMed: 21416623]
42. Ramamurthy S, Chang E, Cao Y, Zhu J, Ronnett GV. AMPK Activation Regulates Neuronal Structure in Developing Hippocampal Neurons. Neuroscience. 2014; 259:13–24. [PubMed: 24295634]
43. Zhou Z, et al. Photoactivated adenylyl cyclase (PAC) reveals novel mechanisms underlying cAMP-dependent axonal morphogenesis. Scientific Reports. 2016; 5:19679. [PubMed: 26795422]
44. Zhong H, et al. Subcellular dynamics of type II PKA in neurons. Neuron. 2009; 62:363–374. [PubMed: 19447092]
45. Diering GH, Gustina AS, Huganir RL. PKA-GluA1 coupling via AKAP5 controls AMPA receptor phosphorylation and cell-surface targeting during bidirectional homeostatic plasticity. Neuron. 2014; 84:790–805. [PubMed: 25451194]
46. Deming PB, et al. Anchoring of Protein Kinase A by ERM (ezrin-radixin-moesin) proteins is required for proper netrin signaling through DCC (deleted in colorectal cancer). Journal of Biological Chemistry. 2015
47. Dodge-Kafka KL, et al. The protein kinase A anchoring protein mAKAP coordinates two integrated cAMP effector pathways. Nature. 2005; 437:574–578. [PubMed: 16177794]

48. Terrin A, et al. PKA and PDE4D3 anchoring to AKAP9 provides distinct regulation of cAMP signals at the centrosome. The Journal of Cell Biology. 2012; 198:607–621. [PubMed: 22908311]
49. Gelman IH, Tombler E, Vargas J. A Role for SSeCKS, a Major Protein Kinase C Substrate with Tumour Suppressor Activity, in Cytoskeletal Architecture, Formation of Migratory Processes, and Cell Migration During Embryogenesis. The Histochemical Journal. 2000; 32:13–26. [PubMed: 10805381]
50. Piontek J, Brandt R. Differential and regulated binding of cAMP-dependent protein kinase and protein kinase C isoenzymes to gravin in human model neurons: Evidence that gravin provides a dynamic platform for the localization for kinases during neuronal development. J Biol Chem. 2003; 278:38970–38979. [PubMed: 12857743]
51. Vardjan N, Kreft M, Zorec R. Dynamics of β-adrenergic/cAMP signaling and morphological changes in cultured astrocytes. Glia. 2014; 62:566–579. [PubMed: 24464905]
52. Soderling SH, et al. Loss of WAVE-1 causes sensorimotor retardation and reduced learning and memory in mice. Proceedings of the National Academy of Sciences of the United States of America. 2003; 100:1723–1728. [PubMed: 12578964]
53. Kawano Y, et al. CRMP-2 is involved in kinesin-1-dependent transport of the Sra-1/WAVE1 complex and axon formation. Mol Cell Biol. 2005; 25:9920–9935. [PubMed: 16260607]
54. Wang Y, et al. Muscle A-Kinase Anchoring Protein-α is an Injury-Specific Signaling Scaffold Required for Neurotrophic- and Cyclic Adenosine Monophosphate-Mediated Survival. EBioMedicine. 2015; 2:1880–1887. [PubMed: 26844267]
55. Lipscombe D, et al. Imaging of cytosolic Ca2+ transients arising from Ca2+ stores and Ca2+ channels in sympathetic neurons. Neuron. 1988; 1:355–365. [PubMed: 2856095]
56. Willoughby D, Wachten S, Masada N, Cooper DM. Direct demonstration of discrete Ca2+ microdomains associated with different isoforms of adenylyl cyclase. J Cell Sci. 2010; 123:107–117. [PubMed: 20016071]
57. Yang JH, Polanowska-Grabowska RK, Smith JS, Shields CWt, Saucerman JJ. PKA catalytic subunit compartmentation regulates contractile and hypertrophic responses to beta-adrenergic signaling. Journal of molecular and cellular cardiology. 2014; 66:83–93. [PubMed: 24225179]
58. Yonaha M, Chibazakura T, Kitajima S, Yasukochi Y. Cell cycle-dependent regulation of RNA polymerase II basal transcription activity. Nucleic Acids Res. 1995; 23:4050–4054. [PubMed: 7479063]
59. Dodge-Kafka KL, et al. The protein kinase A anchoring protein mAKAP coordinates two integrated cAMP effector pathways. Nature. 2005; 437:574–578. [PubMed: 16177794]
60. Kleman AM, Yuan JY, Aja S, Ronnett GV, Landree LE. Physiological Glucose is Critical for Optimized Neuronal Viability and AMPK Responsiveness In Vitro. Journal of neuroscience methods. 2008; 167:292–301. [PubMed: 17936912]

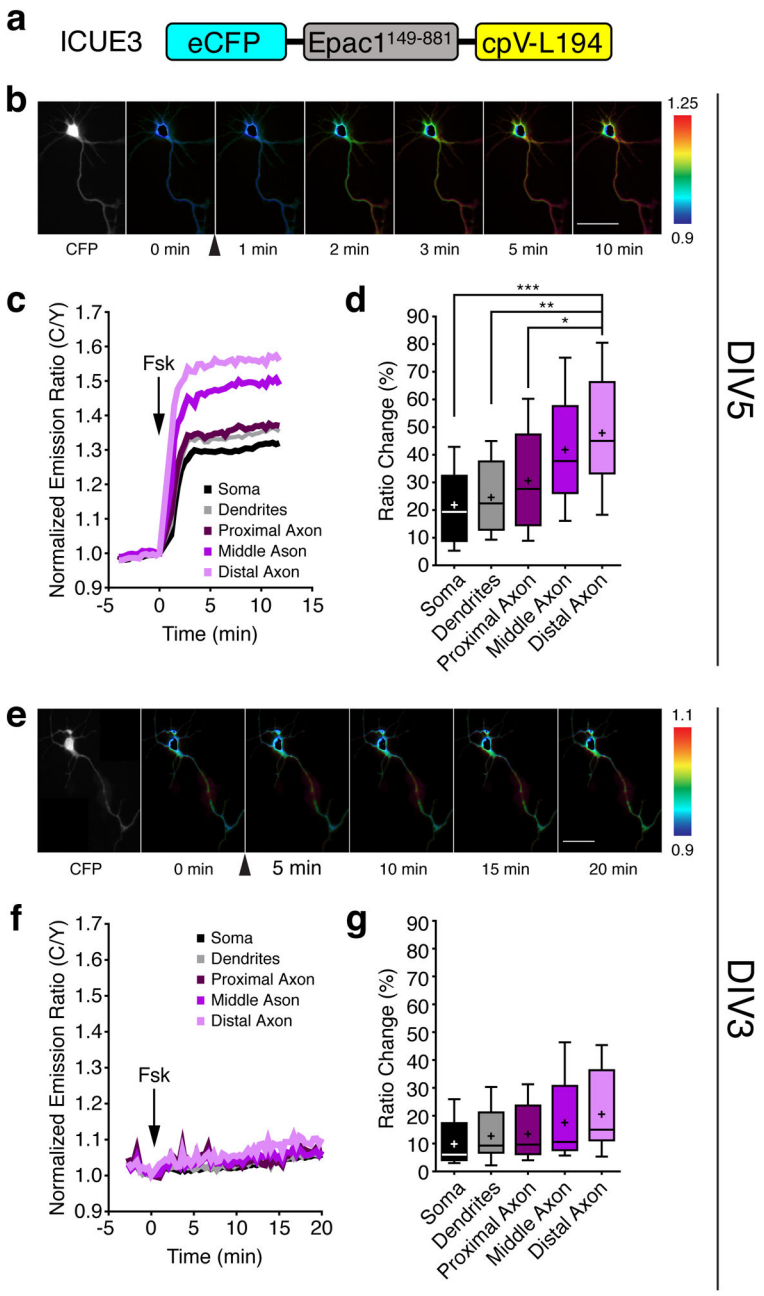

Figure 1.

Spatial regulation of cAMP production in early polarized hippocampal neurons.

(a) Domains of ICUE3, which uses Epac1$^{149–881}$ as the sensing domain and eCFP/cpV-L194 as the FRET pair. (b) Pseudocolored images showing responses of ICUE3 to 50 μM Fsk in a DIV5 HN. Arrowhead indicates drug addition. Warmer colors correspond to higher cyan/yellow (C/Y) emission ratios. (c) Representative time-course of the ratio changes in the soma, dendrites, proximal axon, middle axon, and distal axon from a. (d) Average ICUE3 responses induced by Fsk stimulation (n=12, five preparations; *p=0.032, **p=0.0023, and ***p=0.0009, two-tailed Student's t-test). (e) Pseudocolored images showing the responses

of ICUE3 to 50 μM Fsk in the DIV3 HN. Arrowhead indicates drug addition. Warmer colors correspond to higher C/Y emission ratios. (f) Representative time-course of the ratio changes in the different regions in response to 50 μM Fsk from panel e. (g) Average cAMP increase induced by Fsk stimulation in each region (n=8, three preparations). Data in d and g are shown as box-and-whisker plots, with the box showing the median, 25% quartile, and 75% quartile, and the whiskers designating the 5th and 95th percentiles; a "+" indicates the mean. ns, not significant. Scale bars, 50 μm.

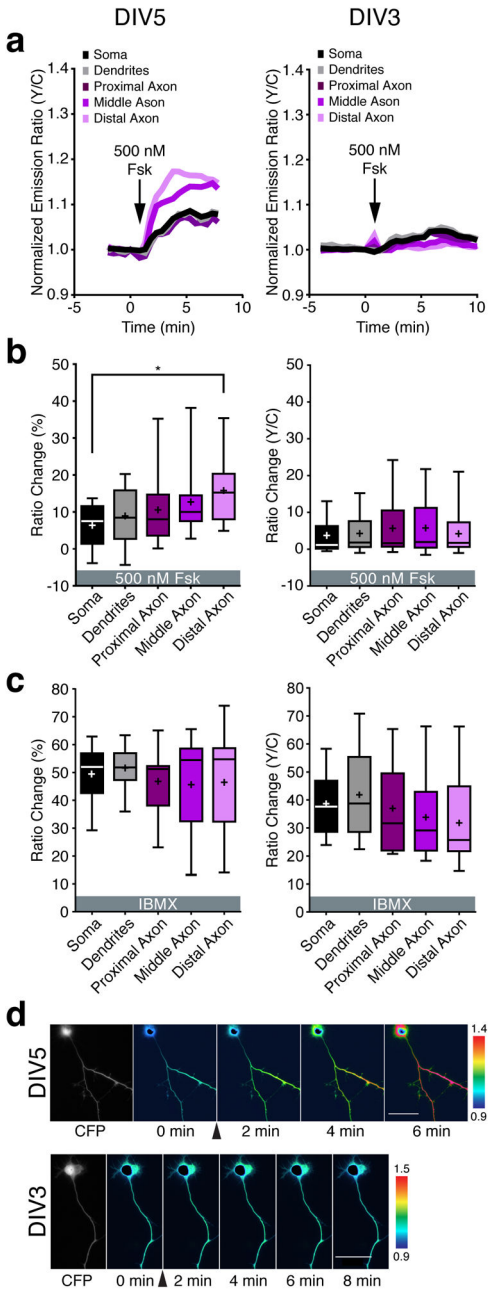

Figure 2.

Spatial regulation of PKA activity in early polarized hippocampal neurons.

(a) Representative time-course of the AKAR4 emission ratio changes in the different compartments of a DIV5 (left) and DIV3 HN (right) in response to 500 nM Fsk. (b) Average AKAR4 responses induced by 500 nM Fsk in DIV5 (left, n=10 from four preparations; *p=0.012 according to two-tailed Student's t-test) and DIV3 HNs (right, n=14 from three preparations). (c) Average AKAR4 response induced by 100 μM IBMX in DIV5 HNs (left, n=9, from three preparations) and 100 μM IBMX followed by 500 nM Fsk in DIV3 HNs (right, n=15 from three preparations). (d) Pseudocolored images showing the responses of

AKAR4 to 500 nM Fsk in the DIV5 (top) and DIV3 (bottom) HN from panel a. Arrowheads indicate the time of drug addition. Warmer colors correspond to higher yellow/cyan (Y/C) emission ratios. Scale bar, 50 μm. Data in b and c are shown as box-and-whisker plots, with the box showing the median, 25% quartile, and 75% quartile, and the whiskers designating the 5th and 95th percentiles; a "+" indicates the mean. ns, not significant.

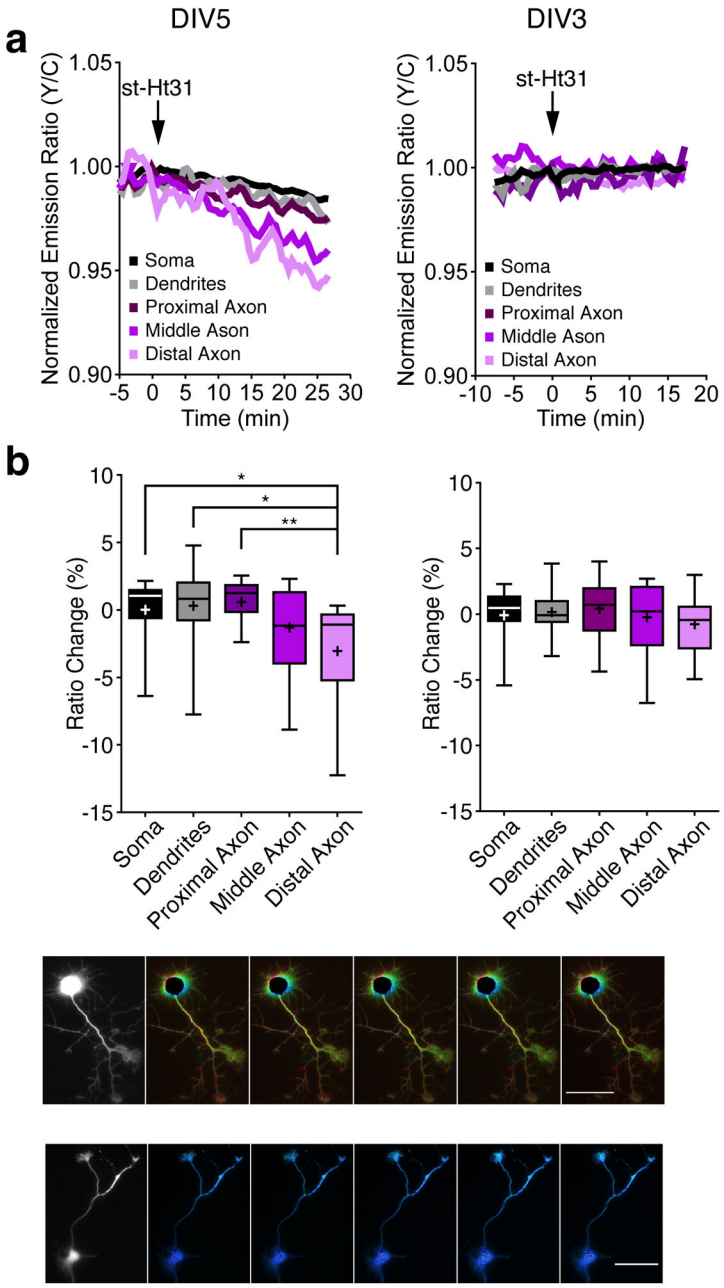

Figure 3.

Acute disruption of AKAP anchoring decreases PKA activity in the axon.

(a) Representative time-course of the AKAR4 emission ratio changes of a DIV5 (left) and DIV3 HN (right) in response to 10 μM st-Ht31. (b) Average AKAR4 response induced by 10 μM st-Ht31 in DIV5 (left, n=15 from three preparations; Distal vs Soma *p=0.012, Distal vs Dendrites *p=0.011, and Distal vs Proximal **p=0.0017 according to two-tailed Student's t-test) and DIV3 HNs (right, n=16 from three preparations). (c) Pseudocolored images showing the responses of AKAR4 to 10 μM st-Ht31 in the DIV5 (top) or DIV3 (bottom) HN from panel a. Arrowheads indicate the time of drug addition. Warmer colors correspond to

higher Y/C emission ratios. Scale bar, 50 μm. Data in b are shown as box-and-whisker plots, with the box showing the median, 25% quartile, and 75% quartile, and the whiskers designating the 5th and 95th percentiles; a “+” indicates the mean. ns, not significant.

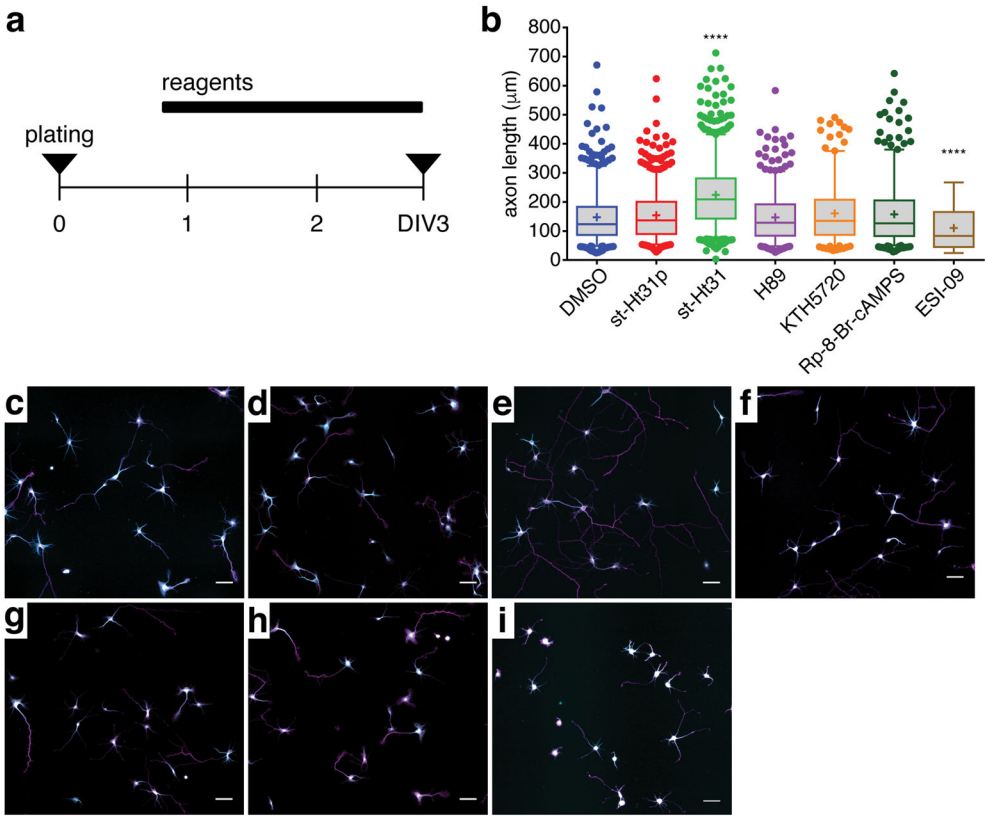

Figure 4.

Disruption of AKAP anchoring increases axon outgrowth in undifferentiated HNs. (a) Schematic of experimental design: newly plated cells (DIV0) were treated with various compounds after ~16 h in vitro. HNs were then fixed at DIV3 for immunostaining. (b) Box-and-whisker plots summarizing the axon length following the indicated treatments. The box shows the median, 25% quartile, and 75% quartile, and the whiskers designate the 5th and 95th percentiles; a "+" indicates the mean. Each bar contains pooled data from at least 170 cells and three preparations. ****$p<0.0001$ vs. DMSO according to two-tailed Student's t-test. (c–i) Representative images of DIV3 HNs immunolabeled with Tau1 (magenta) and MAP2 (cyan) and treated for ~48 h with (c) DMSO, (d) 20 μM st-Ht31p, (e) 20 μM st-Ht31, (f) 10 μM H89, (g) 400 nM KT5720, (h) 200 μM Rp-8-Br-cAMPS, and (i) 15 μM ESI-09. Scale bar, 50 μm.

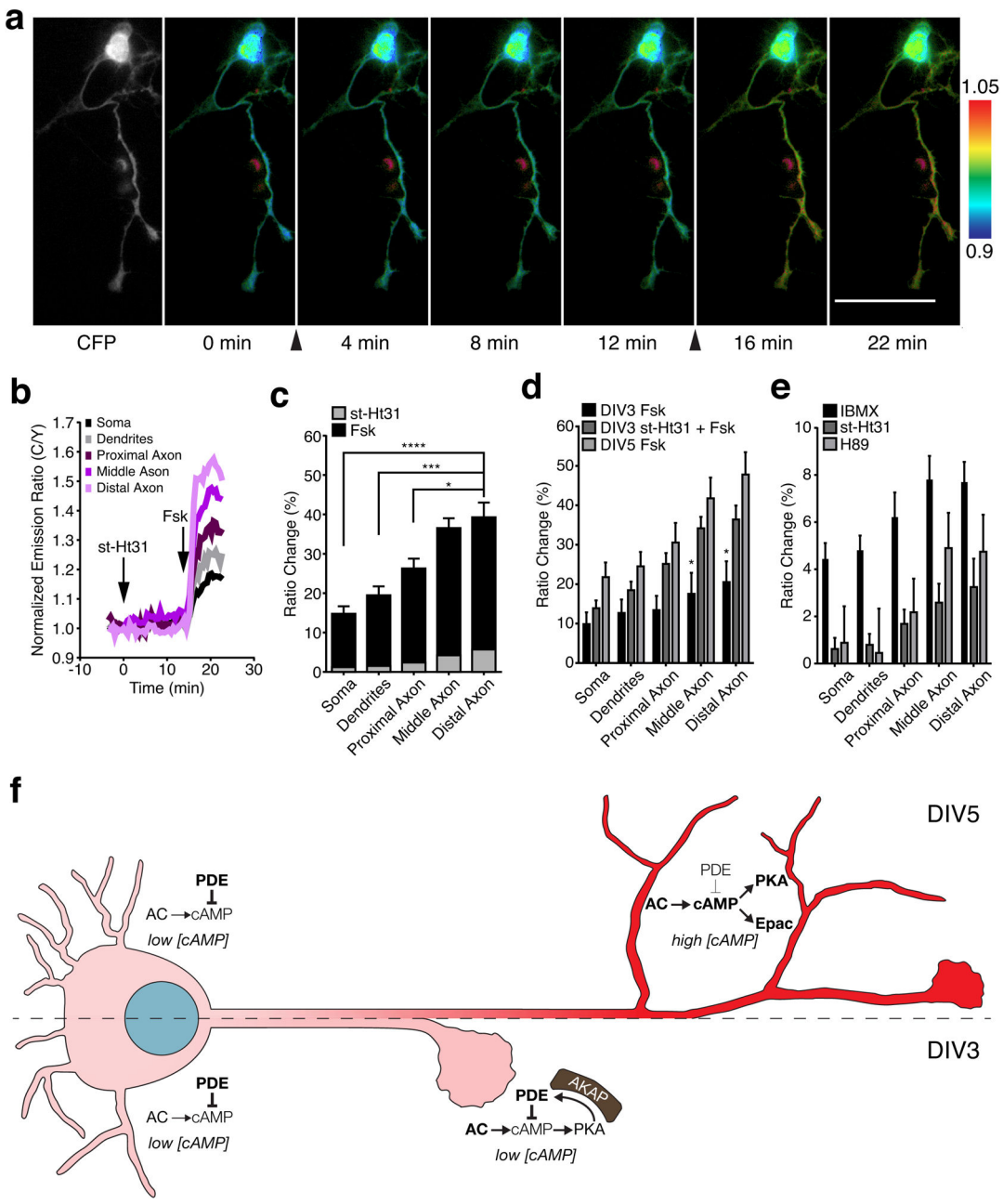

Figure 5.

Acute disruption of AKAP anchoring increases cAMP and reveals an axon-directed cAMP gradient in developing HNs.

(a, b) Pseudocolored images (a) and representative time-course (b) of an ICUE3-expressing DIV3 HN responding to 10 μM st-Ht31 followed by 50 μM Fsk. Arrows indicate drug addition. (c) Stacked comparison of ICUE3 response to st-Ht31 (striped bars) and Fsk (black bars) (n=11, three preparations; *p=0.0231, ***p=0.0006, ****p<0.0001, two-tailed Student's t-test). (d) Comparison of ICUE3 responses in Fsk-treated DIV3 HNs with (black bars, n=8, three preparations) and without (striped bars, n=11 from three preparations) st-

Ht31 pretreatment and in Fsk-treated DIV5 HNs (gray bars, n=12, data reproduced from Fig. 1d). *p<0.05 versus DIV3 HNs treated with both st-Ht31 and Fsk according to two-way ANOVA followed by Dunnett's multiple comparisons test. (e) ICUE3 response to IBMX (n=18, three preparations), st-Ht31 (n=11, three preparations), and H89 (n=9, three preparations) in DIV3 HNs. Bars in c–e represent mean±S.E.M. Scale bars, 50 μm (f) Model of compartmentalized cAMP signaling in developing HNs. In early-stage cells (e.g., DIV3, left), high PDE activity in the soma keeps [cAMP] low, while AKAP-mediated PKA-PDE feedback dampens [cAMP] in the distal axon, thereby restraining axon outgrowth. At later stages (e.g., DIV5, right), high PDE activity continues to maintain low [cAMP] in the soma, whereas the absence of PKA-mediated negative feedback in the axon enables the formation of a steep [cAMP] gradient, with the highest [cAMP] in the distal axon, leading to the activation of downstream effectors such as Epac and PKA, which regulate axon growth. Red coloring indicates cAMP levels.